frontiers | Frontiers in Medicine

TYPE Original Research
PUBLISHED 12 March 2025
DOI 10.3389/fmed.2025.1549491

Check for updates

OPEN ACCESS

EDITED BY
Donglin Di,
Li Auto, China

REVIEWED BY
Hai Guo,
Dalian University, China
Wang Zhendong,
Jiangxi University of Science and Technology, China

*CORRESPONDENCE
Fengbin Zhang
✉ zhangfengbin@hrbust.edu.cn

RECEIVED 21 December 2024
ACCEPTED 25 February 2025
PUBLISHED 12 March 2025

CITATION
Tian C and Zhang F (2025) EEG-based epilepsy detection with graph correlation analysis. *Front. Med.* 12:1549491. doi: 10.3389/fmed.2025.1549491

COPYRIGHT
© 2025 Tian and Zhang. This is an open-access article distributed under the terms of the Creative Commons Attribution License (CC BY). The use, distribution or reproduction in other forums is permitted, provided the original author(s) and the copyright owner(s) are credited and that the original publication in this journal is cited, in accordance with accepted academic practice. No use, distribution or reproduction is permitted which does not comply with these terms.

EEG-based epilepsy detection with graph correlation analysis

Chongrui Tian[1,2] and Fengbin Zhang[1]*

[1]School of Computer Science and Technology, Harbin University of Science and Technology, Harbin, China, [2]School of Information Engineering, East University of Heilongjiang, Harbin, China

Recognizing epilepsy through neurophysiological signals, such as the electroencephalogram (EEG), could provide a reliable method for epilepsy detection. Existing methods primarily extract effective features by capturing the time-frequency relationships of EEG signals but overlook the correlations between EEG signals. Intuitively, certain channel signals exhibit weaker correlations with other channels compared to the normal state. Based on this insight, we propose an EEG-based epilepsy detection method with graph correlation analysis (EEG-GCA), by detecting abnormal channels and segments based on the analysis of inter-channel correlations. Specifically, we employ a graph neural network (GNN) with weight sharing to capture target channel information and aggregate information from neighboring channels. Subsequently, Kullback-Leibler (KL) divergence regularization is used to align the distributions of target channel information and neighbor channel information. Finally, in the testing phase, anomalies in channels and segments are detected by measuring the correlation between the two views. The proposed method is the only one in the field that does not require access to seizure data during the training phase. It introduces a new state-of-the-art method in the field and outperforms all relevant supervised methods. Experimental results have shown that EEG-GCA can indeed accurately estimate epilepsy detection.

KEYWORDS

electroencephalogram, graph neural networks, correlation analysis, anomaly detection, abnormal EEG channels detection

1 Introduction

The field of affective computing has witnessed significant development, drawing attention to emotion detection, especially in medical research related to epilepsy (1). While epilepsy, as a neurological disorder, manifests symptoms that encompass seizures, it often intertwines with fluctuations in emotional states. These emotional variations, a common symptom in epilepsy patients, are crucial for accurate disease monitoring and treatment (2).

Scalp electroencephalogram (EEG) stands as the primary tool for detecting seizures, capturing voltage changes between electrodes and providing spatial-temporal insights into brain activity (3–5). However, the current approach to seizure detection in EEGs relies on manual examination by experienced EEG readers, demanding substantial time and effort. Furthermore, discrepancies in diagnostic results may emerge due to varying opinions among experts (6).

To address these challenges, there is a pressing need for the development of automated and objective methods for epileptic seizure detection. While many studies have proposed deep learning (DL)-based models for automated seizure detection, several challenges persist (7–9). These models often train in a supervised approach, necessitating labeled seizure data that is both scarce and labor-intensive to obtain in real-world applications. Additionally, existing models frequently apply deep convolutional neural networks (CNNs) directly to time-series signals or spectrograms, overlooking crucial information related to physical distance-based and functional-based connectivity between different brain regions (10).

Recent studies have introduced graph learning techniques to capture relationships between EEG electrodes (i.e., EEG nodes) (6, 11, 12). However, these approaches fall short in considering local patterns, such as local sub-graphs and sub-structures, when learning EEG graphs. The inclusion of such local information could prove effective in detecting anomalies in EEG graphs, as demonstrated in other network analysis applications. In real-world applications, an imbalance in data availability between seizure and normal classes is common. Graph-based methods addressing this issue often employ graph augmentation, but not every augmentation technique is effective in EEG graphs (10), as some may compromise underlying brain region connectivities. Therefore, identifying appropriate augmentation strategies in EEG graphs that preserve semantic information is crucial for accurate seizure detection and localization (13).

This study delves into detecting the anomaly channels of EEG signal in patients with epilepsy (14). We propose an innovative method for epilepsy detection that distinctively focuses on exploring the inter-channel relationships within EEG signals, deemed essential for understanding the patient signal variations. We introduce an anomaly detection approach for EEG channels and segments based on inter-channel correlation analysis. This method utilizes Graph Neural Networks (GNNs) (15, 16) to capture the correlation between different channels, providing a more accurate reflection of anomaly changes. To achieve precise detection of anomaly channels in an EEG signal, we propose an EEG-based epilepsy detection method with graph correlation analysis (EEG-GCA), employing a weight-sharing GNN and aligning different channel information distributions with Kullback-Leibler (KL) (17) divergence regularization. During the testing phase, we detect anomalous channels and segments by measuring the correlation between two views, thereby achieving sensitive identification of abnormalities in epilepsy. Notably, our proposed method not only performs well in experiments but is also the only training approach that does not require access to seizure data. This research holds practical significance in improving the effectiveness of epilepsy patient treatment.

- We proposed a method named EEG-GCA for inter-channel correlation analysis simulating the correlation between channels in EEG, revealing subtle differences in patient anomaly changes. This algorithm provides a new approach to EEG signal processing.
- We redefined the anomaly channel detection of EEG as the correlation between channel feature distribution and their neighbors' distribution, and we designed an Unsupervised model to verify the effectiveness.
- The performance evaluation of the proposed abnormal EEG node and region detection is conducted on the extensive and comprehensive EEG seizure dataset TUSZ. The results demonstrate that EEG-GCA sets a new benchmark, achieving state-of-the-art performance on this dataset.

2 Related works

2.1 EEG analysis

Electroencephalogram analysis has become one of the prominent directions (18, 19). The following is a review of relevant work in this field, focusing on the application of different methods and technologies.

(a) Early approaches to epilepsy recognition primarily relied on traditional feature extraction techniques combined with machine learning algorithms (20, 21). Researchers extracted features from different domains, including time-domain, frequency-domain, and time-frequency-domain features, such as power spectral density and energy, to capture epilepsy-related patterns from EEG signals (22). Common machine learning models used in these early approaches included support vector machines (SVM) and decision trees (23, 24). While these methods achieved some success, their performance was often limited by the challenges of manually extracting relevant features and their inability to fully capture the complex dynamics of EEG signals.

(b) In recent years, deep learning methods have gained significant attention for their ability to enhance EEG-based epilepsy recognition (25). Architectures such as convolutional neural networks (CNNs) (26, 27) and recurrent neural networks (RNNs) (28) have been successfully applied, allowing models to learn feature representations in an end-to-end fashion. These deep learning techniques excel at capturing abstract and complex features from the raw EEG signals, significantly improving the accuracy of epilepsy recognition (24, 29). Furthermore, techniques such as transfer learning and multimodal fusion have been extensively explored to improve the generalization capabilities of these models, enabling better performance on unseen data.

(c) Beyond EEG signals, there has been growing interest in integrating data from multiple modalities for epilepsy recognition tasks, including physiological signals, speech, and images (30). Cross-modal research aims to combine information from diverse sources, thereby enhancing the robustness and comprehensiveness of epilepsy detection systems (31, 32). This approach leverages complementary data to improve model performance, offering a more holistic view of the patient's condition and enhancing the reliability of diagnosis (33).

2.2 Canonical correlation analysis

Canonical correlation analysis (CCA) (34, 35) is a method that aims to find the linear transformation for measuring the relationship between two vectors. Give two vectors $\mathbf{X}_1$ and $\mathbf{X}_2$, the

correlation $\rho = \frac{\mathbf{a}^T \Sigma_{\mathbf{X}_1\mathbf{X}_2} \mathbf{b}}{\sqrt{\mathbf{a}^T \Sigma_{\mathbf{X}_1\mathbf{X}_1} \mathbf{a}} \sqrt{\mathbf{b}^T \Sigma_{\mathbf{X}_2\mathbf{X}_2} \mathbf{b}}}$ is maximized by optimizing the objective :

$$\max_{\mathbf{a},\mathbf{b}} \mathbf{a}^T \Sigma_{\mathbf{X}_1\mathbf{X}_2} \mathbf{b}, s.t. \mathbf{a}^T \Sigma_{\mathbf{X}_1\mathbf{X}_1} \mathbf{a} = \mathbf{b}^T \Sigma_{\mathbf{X}_2\mathbf{X}_2} \mathbf{b} = \mathbf{I} \tag{1}$$

Soft-CCA (36) considers the decorrelation constraint as a term of loss and optimizes it jointly with other terms, and the objective of Soft CCA is:

$$\begin{aligned} &\max_{\theta 1,\theta 2} Tr(P_{\theta_1}^T(\mathbf{X}_1) P_{\theta_2}(\mathbf{X}_2)) \\ &s.t. P_{\theta_1}^T(\mathbf{X}_1) P_{\theta_1}(\mathbf{X}_1) = P_{\theta_2}^T(\mathbf{X}_2) P_{\theta_2}(\mathbf{X}_2) = \mathbf{I} \end{aligned} \tag{2}$$

where $\mathbf{I}$ is the identity matrix, and Equation 2 can be rewritten as:

$$\begin{aligned} &\min_{\theta 1,\theta 2} ||P_{\theta_1}(\mathbf{X}_1) - P_{\theta_2}(\mathbf{X}_2)||_F^2 + \\ &\lambda(\mathcal{L}_{SDL}(P_{\theta_1}(\mathbf{X}_1)) + \mathcal{L}_{SDL}(P_{\theta_2}(\mathbf{X}_2))) \end{aligned} \tag{3}$$

where P_{θ_1} and P_{θ_2} are the neural networks used to learn the representations of the two views. $||P_{\theta_1}(\mathbf{X}_1) - P_{\theta_2}(\mathbf{X}_2)||_F^2$ is used to maximize the correlation between the two views, and $\mathcal{L}_{SDL}$ is used to minimize the distance between $P_{\theta_i}(\mathbf{X}_i)$ and the identity matrix.

2.3 Graph learning methods

Graph data, being non-Euclidean, poses a challenge for traditional convolution methods. The effective learning of information from graph data is an actively researched problem (37). In the context of graph data, the learned representation of nodes should encapsulate both the structural information of the graph and the attributes associated with each node. Existing graph learning methods can be broadly categorized as follows:

Truncated Random Walk-Based Methods: These methods operate on the assumption that nodes with similar network structures should have similar vector representations. A notable approach in this category is DeepWalk (38), which employs random walks to generate training data and leverages Word2vec (39) to learn node representations. Node2vec (40) captures homogeneity and structural equivalence through weighted random walks.

Methods Based on k-Order Distance Between Nodes in the Graph: These approaches, exemplified by methods like LINE (41) and GraRep (42), learn node representations by capturing k-order relational structure information, aiming to achieve high-quality node embeddings.

Deep Learning-Based Methods: Distinguished by their use of deep learning, these methods (43, 44) leverage the advantages of deep neural networks to extract high-order nonlinear relationships from graph data.

Graph neural networks (GNNs) (45) represent a significant advancement as they directly operate on graph data, aggregating each node's features with those of its neighbors. Building on GNNs, certain methods (46, 47) utilize GNNs to learn node representations. They employ adversarial learning to regularize these representations and predict the likelihood of an edge existing between a pair of nodes. However, these approaches predominantly rely on graph structure information.

Moreover, methods based on dual-autoencoders, such as AnomalyDAE (45) and Dual-SVDAE (48), use Graph Convolutional Networks to capture graph structure information. They combine this with multi-layer perceptrons (MLPs) to capture node attribute information, thereby making full use of attribute network information.

3 Method

In this section, we detail the EEG-GCA in Figure 1. It consists of a graph construct module, the information mining model, and a correlation analysis module. At first, we construct the EEG graph as input for our model. Then, we introduce an identity graph that represents the identity matrix, signifying no relationships between the channels. This graph aims to capture the features of each channel in the EEG data. Then, we input the EEG graph and identity graph into a weight-sharing GCN to learn the distribution of structural information and distribution of semantic information and pull the distributions to the same prior distribution through the Kullback-Leibler (KL) divergence. Finally, we sample the network structure embedding and node embedding from the learned distribution and maximize the correlation of normal nodes on the network structure distribution and node attribute distribution by using the CCA-based objective. The correlation score is used to detect the anomaly channels.

3.1 EEG graph construction

In this paper, we first construct the EEG graph as input. The EEG graph can be defined as an attributed network $\mathcal{G} = \{\mathbf{A}, \mathbf{X}\}$. Where $\mathbf{A} \in \mathbb{R}^{N \times N}$ is the adjacency matrix that denotes the connection between each electrode. $\mathbf{X} \in \mathbb{R}^{N \times D}$ denotes the feature matrix. $\mathbf{X}_i$ is feature of the i-th channel. Similar to the study, given an EEG clip, we construct five types of EEG graphs (12).

- *Dist − EEG − Graph* strives to embed the structure of electrode locations in the graph's adjacency matrix by leveraging the Euclidean distance between electrodes. Given that electrode locations remain fixed within an EEG recording cap, the same adjacency matrix is applied to all EEG clips. More precisely, the elements a_{ij} of the Dist-EEG-Graph are computed as follows:

$$a_{ij} = \begin{cases} \exp(-\frac{||v_i - v_j||}{\tau^2}), & if\ ||v_i - v_j||^2 \leq k, \\ 0, & if\ O.W. \end{cases} \tag{4}$$

  Here, $||\bullet||$represents the l_2-norm, and τ is a scaling constant. The proximity between two electrodes, v_i and v_j, is reflected by the proximity of a_{ij} to 1. In this paper, k is uniformly set to 0.9 across all EEG clips. Assigning a value of 0 to a_{ij} for distant electrodes introduces sparsity to the graph.
- *Corr − EEG − Graph* The purpose of this graph is to capture the functional connectivity between electrodes, which is encoded

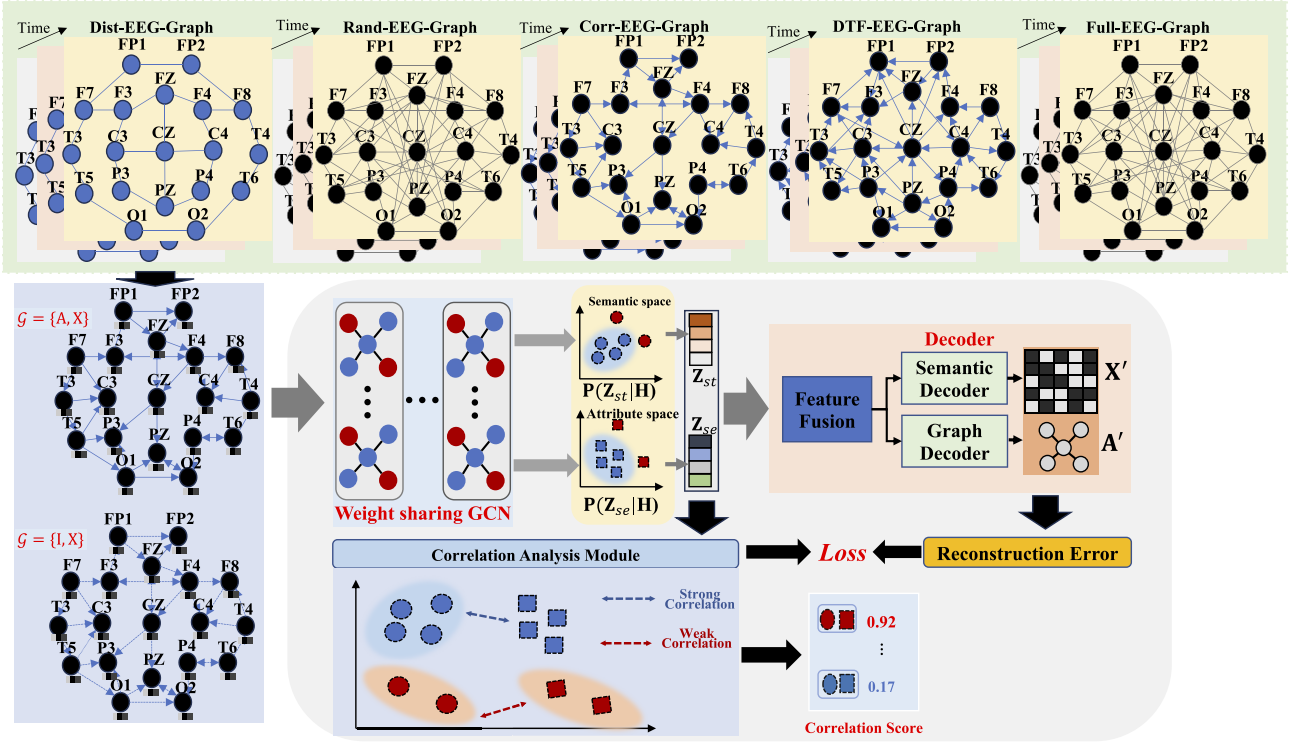

FIGURE 1
The framework of the proposed EGG-GCA.

in the elements of the adjacency matrix defined as follows:

$$a_{ij} = \begin{cases} \frac{corr(\mathbf{X}_i,\mathbf{X}_j)}{||\mathbf{X}_i||||\mathbf{X}_j||}, & if\ v_j \in \mathcal{N}(v_i), \\ 0, & if\ O.W. \end{cases} \quad (5)$$

where $corr(\bullet)$ denotes the cross-correlation function, and v_i represents the top-3 neighborhood nodes of v_i with the highest normalized correlation. $\mathcal{N}(v_i)$ is set to the top-3 neighborhood nodes to avoid overly connected graphs. Additionally, we only keep the top three edges for each node to prevent excessively connected graphs.

- *Rand − EEG − Graph* The construction of this graph is grounded on the assumption that all electrodes are interconnected and equally contribute to brain activities. The realization of this graph involves the formation of an adjacency matrix according to the following procedure:

$$a_{ij} = \begin{cases} 0.5, & if\ i \neq j, \\ 1, & if\ O.W. \end{cases} \quad (6)$$

- *Full − EEG − Graph* Similar to the *Rand − EEG − Graph*, The construction of this graph is grounded on the assumption that all electrodes are interconnected and equally contribute to brain activities. But the a_{ij} is set as 1 for each connection.
- *DTF − EEG − Graph* The Directed Transfer Function Graph aims to represent the mutual influence between EEG channels, thereby modeling the functional connectivity of different brain regions. The adjacency matrix for this graph is defined as follows:

$$a_{ij} = \begin{cases} \frac{corr(\mathbf{X}_i,\mathbf{X}_j)}{\sqrt{\sum_{m=1,m\neq i,j}^{n}||corr(\mathbf{X}_i,\mathbf{X}_m))||^2}}, & if\ v_j \in \mathcal{N}(v_i), \\ 0, & if\ O.W. \end{cases} \quad (7)$$

3.2 Weight-sharing GCN

To learn the correlation within the weight-sharing Graph Convolutional Network (GCN) for capturing the semantic and structural information of each node, we introduced an identity graph denoted as $\mathcal{G}' = \{\mathrm{I}, \mathrm{X}\}$, where I represents the identity matrix signifying no relationships between the channels. This approach enhances the similarity between the semantic information and the graph structure information of each node by transferring the learned semantic information to all node features. Consequently, each channel feature can be obtained by inputting the identity graph into the Weight-Sharing GCN.

The construct EEG-graph $\mathcal{G}$ explicitly expresses the correlations between the channels in the EEG data, therefore, to capture the relationship information (structural information) between different channels, we input the EEG graph $\mathcal{G} = \{\mathrm{A}, \mathrm{X}\}$ to the weight-sharing GCN.

$$GCN(\mathbf{X}, \mathbf{A}|\boldsymbol{W}) = \varphi((\mathbf{D})^{-\frac{1}{2}}\mathbf{A}(\mathbf{D})^{-\frac{1}{2}}\mathbf{X}\boldsymbol{W}) \quad (8)$$

where $\boldsymbol{W}$ is the learnable sharing weight, φ is activation function, and $\mathbf{D}$ is the diagonal degree matrix of the constructed EEG graph $\mathcal{G}$.

To extract each channel information (node semantic information), the identity aggregation is designed which inputs the identity graph $\mathcal{G}^{'} = \{\mathrm{I}, \mathrm{X}\}$ to the weight-sharing GCN:

$$GCN(\mathbf{X}, \mathbf{I}|\boldsymbol{W}) = \varphi(\mathbf{I}\mathbf{X}\boldsymbol{W}) \tag{9}$$

3.3 Distribution alignment

After obtain the node structural information embedding $\mathbf{Z}_{st}$ and the node semantic information embedding $\mathbf{Z}_{se}$, we capture the structural distribution $q(\mathbf{Z}_{st}|\mathbf{X}, \mathbf{A})$ and semantic distribution $q(\mathbf{Z}_{se}|\mathbf{X}, \mathbf{I})$ for each node by Equation 10, respectively.

$$q(\mathbf{Z}|\mathbf{X}, \mathbf{A}) = \prod_{i=0}^{N} q(\mathbf{z}_i|\mathbf{X}, \mathbf{A}) \tag{10}$$

$$q(\mathbf{z}_i|\mathbf{X}, \mathbf{A}) = \mathcal{N}(\mathbf{z}_i|\boldsymbol{\mu}_i, \mathrm{diag}(\boldsymbol{\sigma}^2)) \tag{11}$$

where $\mathbf{Z}$ is the embedding sampled from the distribution. $\boldsymbol{\mu}$ is the mean vector and $\boldsymbol{\sigma}$ is the variance vector, which is learned by two different GCN layers.

$$\boldsymbol{\mu} = \mathrm{GCN}_{\boldsymbol{\mu}}(\mathbf{H}, \mathbf{A}|\boldsymbol{W}) \tag{12}$$

$$\boldsymbol{\sigma} = \mathrm{GCN}_{\boldsymbol{\sigma}}(\mathbf{H}, \mathbf{A}|\boldsymbol{W}) \tag{13}$$

where $\boldsymbol{\mu}_h$ and $\boldsymbol{\sigma}_h$ denote the mean and variance vectors of the structural distribution learned by Equations 12, 13. Similarly, $\boldsymbol{\mu}_f$ and $\boldsymbol{\sigma}_f$ are the mean and variance vectors of semantic distribution learned by Equations 12, 13.

To capture the correlation between the two distributions, we should align the structural distribution and semantic distribution. Due to it being harder to directly align two distributions, we use a Gaussian distribution as prior distribution p and use Kullback-Leibler (KL) divergence to align the two distributions wanting this prior distribution to achieve the desired effect.

$$\mathcal{L}_{kl} = -\mathrm{KL}[q(\mathbf{Z}_{st}|\mathbf{X}, \mathbf{A})||p(\mathbf{Z}_{st})] - \mathrm{KL}[q(\mathbf{Z}_{se}|\mathbf{X}, \mathbf{I})||p(\mathbf{Z}_{se})] \tag{14}$$

3.4 Decoder

The reconstruction of graph data is divided into two main parts, the reconstruction of the network structure and the reconstruction of the node attributes. Since nodes in graph data often have complex interactions with each other, it is necessary to fuse the features of each node with those of their neighbors.

$$\mathbf{Z}_f = \mathbf{Z}_{st} + \mathbf{Z}_{se} \tag{15}$$

Then we use an L-layers Multi-Layer Perceptron (MLP) to reconstruct the node attributes.

$$\mathbf{Z}_f^{(l)} = \sigma(\mathbf{Z}_f^{(l-1)}\mathrm{W}^{(l-1)} + \mathbf{b}^{(l-1)}) \tag{16}$$

where $\mathbf{Z}_f^{(l-1)}$, $\mathbf{Z}^{(l)}$, $\mathbf{W}^{(l-1)}$ and $\mathbf{b}^{(l-1)}$ are the input, output, the trainable weight and bias matrix of $(l-1)$-th layer respectively, $l \in \{1, 2, ..., L\}$. $\sigma(\bullet)$ is the activation function. Finally, the reconstruction of node attributes $\hat{\mathbf{X}} = \mathbf{Z}_f^{(L)}$ is obtained from the output of the last layer in MLP.

For the reconstruction of the network structure, we use an inner production of fusion embedding $\mathbf{Z}_f$ to reconstruct the network structure.

$$\hat{\mathbf{A}} = \mathbf{Z}_f\mathbf{Z}_f^T \tag{17}$$

The reconstruction loss is defined as:

$$\mathcal{L}_{dec} = ||\mathbf{X} - \hat{\mathbf{X}}|| + ||\mathbf{A} - \hat{\mathbf{A}}|| \tag{18}$$

3.5 Correlation analysis objective

The objective of correlation analysis is to discern the relationship between structural distribution and semantic distribution. Initially, we sample the embeddings of structural information, denoted as $\mathbf{Z}st$, and semantic information, denoted as $\mathbf{Z}se$, from the distributions of structural features $q(\mathbf{Z}st|\mathbf{X}, \mathbf{A})$ and semantic features $q(\mathbf{Z}se|\mathbf{X}, \mathbf{I})$. Subsequently, we normalize the node embeddings for the two perspectives using the following procedure.

$$\begin{aligned} \mathbf{Z}_{st}^{'} &= \frac{\mathbf{Z}_{st} - \mu(\mathbf{Z}_{st})}{\sigma(\mathbf{Z}_{st}) * N^{\frac{1}{2}}} \\ \mathbf{Z}_{se}^{'} &= \frac{\mathbf{Z}_{se} - \mu(\mathbf{Z}_{se})}{\sigma(\mathbf{Z}_{se}) * N^{\frac{1}{2}}} \end{aligned} \tag{19}$$

Subsequently, as per the formulation in Equation 3, EEG-GCA enhances the correlation between the distributions of the two views by minimizing the invariance between the network structure embedding $\mathbf{Z}_{st}$ and the node attribute embedding $\mathbf{Z}f$. The invariance loss, denoted as $\mathcal{L}inv$, is defined as:

$$\mathcal{L}_{inv} = ||\mathbf{Z}_{st}^{'} - \mathbf{Z}_{se}^{'}||_F^2 \tag{20}$$

To prevent collapsed solutions, we introduce the decorrelation loss, denoted as $\mathcal{L}_{dco}$, which aims to guarantee that the individual dimensions of the features are uncorrelated.

$$\mathcal{L}_{dco} = ||\mathbf{Z}_{st}^{'T}\mathbf{Z}_{st}^{'} - \mathbf{I}||_F^2 + ||\mathbf{Z}_{se}^{'T}\mathbf{Z}_{se}^{'} - \mathbf{I}||_F^2 \tag{21}$$

The CCA-based objective is defined as follows:

$$\mathcal{L}_{CCA} = \mathcal{L}_{inv} + \lambda * \mathcal{L}_{dco} \tag{22}$$

where λ is the trade-off between the two terms.

3.6 Loss function and anomaly score

The training objective of the proposed model involves optimizing the CCA-based loss along with minimizing the Kullback-Leibler (KL) divergence

TABLE 1 Train and test sets of TUSZ used in the supervised method and unsupervised method.

Data	Patients (% SZ)	EEG files (% SZ)	EEG clips (% SZ)
$Train_{Sup}$	591 (34.0%)	4,599 (18.9%)	38,613 (9.3%)
$Train_{ours}$	493 (0%)	4,028 (0%)	35,019 (0%)
Test	45 (77.8%)	900 (25.6%)	8,848 (14.7%)

The percentages of the seizure data (SZ) is indicated in parenthesis.

between the network structure distribution and the node attribute distribution.

$$\mathcal{L} = \mathcal{L}_{CCA} + \mathcal{L}_{KL} + \mathcal{L}_{dec} \tag{23}$$

The anomaly score is defined as the correlation between channels with their structure information.

4 Performance evaluation

4.1 Dataset

In this study, we employed the Temple University Hospital EEG Seizure Corpus (TUSZ) v1.5.2 (12) as the benchmark dataset. This dataset stands out due to its extensive inclusion of seizure categories and patient samples, making it the dataset with the highest level of variability. Recorded over several years and by different generations of equipment, the dataset covers subjects of all ages, adding to its complexity and rendering it the most challenging for seizure detection. The EEG signals in TUSZ are captured using 19 channels based on the standard EEG 1,020 system. Table 1 provides an overview of the TUSZ dataset utilized in our experiments.

During the training phase, we employed an equal number of normal clips as other supervised methods, omitting any seizure clips. In the testing phase, we utilized an equivalent number of test clips, encompassing both seizure and normal clips, for comparison against other supervised methods and our proposed approach. To assess the model's proficiency in seizure localization, we leveraged available annotations that specify focal and generalized seizure types from 23 distinct patients. It's noteworthy that, in epilepsy patients, focal and generalized seizure types are more prevalent compared to other seizure types, making them particularly relevant for our evaluation.

4.2 Baselines

We conducted a comprehensive evaluation of our proposed EEG-GCA method by comparing it with two distinct streams of deep learning-based approaches (12). The first stream involves well-established DL models operating in the EEG time-series and spectrograms domain, including EEGNet, EEG-TL, Dense-CNN, LSTM, and CNN-LSTM. The second stream focuses on DL models specifically designed for processing EEG graph data. Notably, our method differs from the others as it is deliberately trained without utilizing any seizure data in the training phase, ensuring a fair comparison. In addition, we compared another method, EEG-CGS (12), a graph-based method, which utilizes the constructed EEG graph and self-supervised learning to capture local structural and contextual information embedded in EEG graphs and detects the anomaly by designed anomaly scores.

In this paper, we explore six variations of EEG-GCA based on different input graph types: EEG_d-GCA, EEG_r-GCA, EEG_c-GCA, EEG_f-GCA, EEG_t-GCA, and EEG_l-GCA. These variations utilize Dist-EEG-Graph, Rand-EEG-Graph, Corr-EEG-Graph, Full-EEG-Graph, DTF-EEG-Graph, and Identity-EEG-Graph as their respective inputs. All methods were evaluated on the same dataset, with the comparative analysis focusing on assessing the robustness and generalization capabilities of EEG-GCA, particularly in scenarios where seizure data is limited or unavailable. To evaluate the performance of the models, we used three metrics: Area Under the Curve (AUC), Average Precision (AP), and Specificity (SPC). These metrics provide insights into the models' ability to distinguish between different classes, their precision in detecting positive samples, and their ability to correctly identify negative samples, respectively.

4.3 Detection of seizure clips and channels

The performance of the seizure clip detection experiment across various comparison methods is shown in Table 2. Among the supervised methods, Corr-DCRNN exhibits the highest accuracy of 0.4482, suggesting that it effectively utilizes correlation information between different EEG channels. This is a crucial feature for seizure detection, as it allows the model to capture temporal dependencies and spatial relationships within the EEG signal. However, despite its relatively high accuracy, the model still struggles with achieving high specificity, which is essential for minimizing false positives in seizure detection.

In the unsupervised methods, EEG_r-CGS, based on random graphs, performs the best with an accuracy of 0.4285. This result indicates that even without the use of labeled data, the model is still able to leverage the underlying structure in the EEG data to some extent. However, the performance gap between EEG_r-CGS and supervised methods suggests that unsupervised learning still faces challenges in achieving comparable detection accuracy, particularly when it comes to fine-tuning the decision boundaries between seizure and non-seizure clips.

When comparing our proposed methods–EEG_d-GCA, EEG_r-GCA, EEG_c-GCA, EEG_f-GCA, EEG_t-GCA, and EEG_l-GCA–it is evident that the introduction of the Graph Correlation Attention (GCA) mechanism leads to significant improvements in both accuracy and specificity. The accuracy of our methods consistently outperforms both the supervised and unsupervised methods, with EEG_d-GCA achieving the highest accuracy at 0.6812. This result is particularly noteworthy considering that EEG_d-GCA utilizes the Dist-EEG-Graph as input, which focuses on capturing the structural relationships between different EEG channels. The combination

TABLE 2 Seizure clips detection result.

Method	Acc	Precision	Spec	Method	Acc	Precision	Spec
Supervised				Unsupervised			
EEGNet	0.4742	0.298	0.9021	EEG_d-CGS	0.3076	0.3076	0.9450
EEG-TL	0.4001	0.2675	NA	EEG_r-CGS	0.4285	0.3333	0.9291
Dense-CNN	0.4143	0.2746	0.8692	EEG_c-CGS	0.2857	0.2857	0.9132
LSTM	0.3652	0.2635	0.8143	EEG_f-CGS	0.2857	0.2857	0.9211
CNN-LSTM	0.3304	0.2572	0.8574	EEG_t-CGS	0.3076	0.3076	0.9009
Dist-DCRNN	0.3414	0.2612	0.9321	–	–	–	–
Corr-DCRNN	0.4482	0.2711	0.9003	–	–	–	–
Ours							
EEG_d-GCA	0.6812	0.3469	0.9714	EEG_r-GCA	0.6636	0.3438	0.9429
EEG_c-GCA	0.6847	0.3469	0.9714	EEG_f-GCA	0.6832	0.3469	0.9714
EEG_t-GCA	0.6848	0.3469	0.9714	EEG_l-GCA	0.6625	0.3438	0.9429

of attention mechanisms with graph-based representations allows the model to selectively focus on the most informative features, leading to a more robust and accurate detection of seizure clips.

Interestingly, while EEG_d-GCA achieves the highest accuracy, the other GCA variations (EEG_r-GCA, EEG_c-GCA, EEG_f-GCA, EEG_t-GCA, EEG_l-GCA) also show consistently high performance with accuracy values close to 0.6847. This suggests that the robustness of the GCA mechanism is not highly sensitive to the specific graph input type, which makes these methods versatile across different graph representations of the EEG data. The consistently high specificity of around 0.9714 across all EEG-GCA methods indicates their effectiveness in minimizing false positives, which is a critical factor in the practical application of seizure detection systems.

4.4 Detection of synthetic anomalous channels

In this section, we focus on evaluating the performance of the proposed method EEG-GCA in reliably detecting anomalous channels. To this end, we generate a synthetic test set using normal clips from the training phase. Specifically, we average every 35 normal clips without overlap and then introduce anomalies into the averaged clips with a 3% probability. The anomalies are injected with a 0.03% probability, and at most one node is corrupted per averaged clip. The corruptions are applied both structurally and contextually. The structural corruption involves connecting the selected node to all other nodes in the average clip, while the contextual corruption alters the attribute vector of the node by replacing its feature vector with that of the node in the clip that has the largest Euclidean distance. After introducing these anomalies, we input the averaged clips, some of which contain anomalies, into the EEG-GCA networks that were trained on pure normal clips.

TABLE 3 Synthetic anomalous channels detection results.

Type	Method	AUC	AP	Spec
Supervised	EEGNet	0.6182	0.298	0.902
	EEG-TL	0.5913	0.2675	NA
	Dense-CNN	0.5877	0.2746	0.869
	LSTM	0.5198	0.2635	0.814
	CNN-LSTM	0.5412	0.2572	0.857
	Dist-DCRNN	05683	0.2612	0.932
	Corr-DCRNN	0.6122	0.2711	0.900
Unsupervised	EEG_d-CGS	0.6182	0.0845	0.9455
	EEG_r-CGS	0.8173	0.2675	0.9555
	EEG_c-CGS	0.8241	0.2887	0.9555
	EEG_f-CGS	0.8143	0.2960	0.9555
	EEG_t-CGS	0.8241	0.2887	0.9555
Ours	EEG_d-GCA	0.8903	0.4193	0.9667
	EEG_r-GCA	0.9229	0.4618	0.9722
	EEG_c-GCA	0.916	0.402	0.97
	EEG_f-GCA	0.908	0.4325	0.9689
	EEG_t-GCA	0.9101	0.4172	0.9678
	EEG_l-GCA	0.9238	0.4792	0.9722

The trained system then computes the anomaly scores for all channels.

The experimental results, as summarized in Table 3, demonstrate the effectiveness of our approach in the domain of anomaly detection. Our method outperforms both supervised and other unsupervised learning techniques across key evaluation metrics such as AUC, AP, and Specificity. Specifically, EEGNet, a supervised learning method, achieves a moderate performance with an AUC of 0.6182. However, it faces challenges when

handling imbalanced datasets, which is a critical issue in real-world anomaly detection tasks. In contrast, EEG-GCA demonstrates remarkable improvements in AUC, with EEG_r-GCA and EEG_l-GCA achieving 0.9229 and 0.9238, respectively, highlighting the effectiveness of unsupervised learning techniques in addressing imbalances in the dataset. For AP, EEG-GCA surpasses the performance of the other methods. For instance, EEG_l-GCA reaches an AP of 0.4792, significantly outperforming the supervised approaches. This indicates that our method is highly capable of accurately identifying anomalous events, which is crucial in real-world anomaly detection tasks such as sentiment recognition. Notably, EEG-GCA also excels in terms of Specificity, a metric that measures the ability to correctly identify normal samples and minimize false positives. Both EEG_r-GCA and EEG_l-GCA achieve Specificity values of 0.9722, outperforming all supervised models. This is particularly important as it demonstrates that our method can maintain high sensitivity while effectively reducing false positives, thereby improving the robustness and reliability of anomaly detection.

TABLE 4 Ablation study on seizure clips detection results.

Method	Without correlation			Ours		
	AUC	AP	Spec	AUC	AP	Spec
EEG_d-GCA	0.7579	0.3378	0.9644	0.8903	0.4193	0.9667
EEG_r-GCA	0.8377	0.3431	0.9622	0.9229	0.4618	0.9722
EEG_c-GCA	0.8513	0.4227	0.9678	0.9160	0.4020	0.9700
EEG_f-GCA	0.8628	0.4025	0.9612	0.9080	0.4325	0.9689
EEG_t-GCA	0.8355	0.3489	0.9533	0.9101	0.4172	0.9678
EEG_l-GCA	0.8331	0.3301	0.9622	0.9238	0.4792	0.9722

4.5 Ablation study

In the ablation study for seizure clip detection on synthetic anomalous channels, we explored two distinct approaches: Without Correlation and EEG-GCA. The results of this ablation analysis are summarized in Table 4.

In the Correlation approach, several graph construction methods were employed. Among these, EEG_c-GCA emerged as the top performer, achieving the highest AUC (0.8513) and AP (0.4227), underscoring its effectiveness in seizure detection. This result emphasizes the importance of incorporating correlation in the graph construction process for improving detection accuracy. Notably, EEG_r-GCA and EEG_t-GCA also displayed competitive results, highlighting their resilience to the absence of correlation while still maintaining reasonable performance. These findings suggest that, even without explicit correlation, the models are capable of leveraging other aspects of the data for meaningful detection.

4.6 Visualization of EEG signal

To evaluate the abnormal channels in the electroencephalogram (EEG) segments during epileptic seizures, we visualize the seizure channel for generalized seizures.

In Figure 2, which represents a case of generalized seizures, our method demonstrates a high level of accuracy in detecting all abnormal channels. This robust performance aligns with our expectations for identifying anomalies during generalized seizure events, highlighting the reliability of our approach in such scenarios. The elevated anomaly scores observed in the seizure-affected channels provide strong evidence of the discriminatory power of our model, successfully distinguishing pathological EEG patterns from normal, baseline activity. This

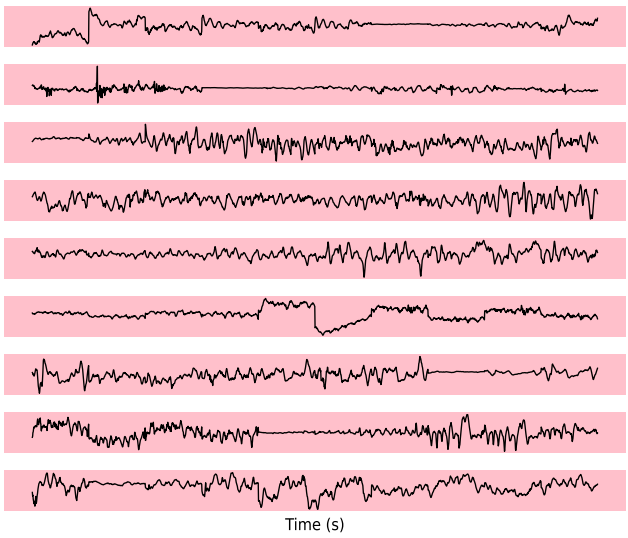

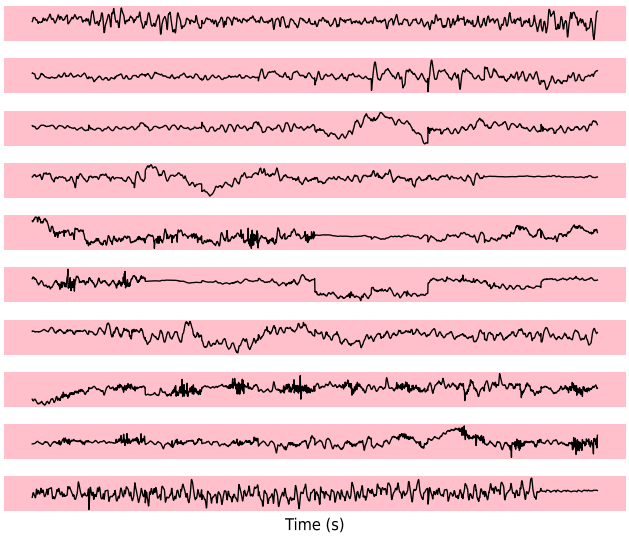

FIGURE 2
The visualization of seizure channel detection for generalized seizures.

underscores the potential of our approach for real-time, accurate seizure detection.

5 Conclusion

In this paper, we introduce EEG-GCA, an unsupervised graph-based model designed for EEG-based epilepsy detection. The core of the methodology is centered around computing the correlation between individual EEG channels and their neighboring channels. The process begins with the construction of a graph representation of the EEG data, which enables the exploration of correlation patterns across the channels. A weight-sharing Graph Convolutional Network is then employed to effectively capture both the semantic and structural relationships among the channels. By aligning these distributions with a prior distribution, EEG-GCA learns the underlying correlations within the EEG data. The final stage involves detecting anomalous channels based on the correlation scores, with weak correlation scores indicating potential anomalies that may signify seizures. The experimental results demonstrate that EEG-GCA outperforms existing methods, achieving superior accuracy in detecting anomalous channels. This underscores the effectiveness of leveraging graph-based correlation techniques for the detection of epilepsy in EEG signals. In the future, we exploration involves integrating multi-modal data, such as incorporating additional physiological signals or patient-specific features, to further enhance the robustness and adaptability of models.

Data availability statement

The original contributions presented in the study are included in the article/supplementary material, further inquiries can be directed to the corresponding author.

Author contributions

CT: Formal analysis, Investigation, Methodology, Software, Writing – original draft. FZ: Funding acquisition, Investigation, Writing – review & editing.

Funding

The author(s) declare that financial support was received for the research and/or publication of this article. This work was supported by the Key R&D Program Guidance Projects in Heilongjiang Province GZ20240040.

Conflict of interest

The authors declare that the research was conducted in the absence of any commercial or financial relationships that could be construed as a potential conflict of interest.

Generative AI statement

The author(s) declare that no Gen AI was used in the creation of this manuscript.

Publisher's note

All claims expressed in this article are solely those of the authors and do not necessarily represent those of their affiliated organizations, or those of the publisher, the editors and the reviewers. Any product that may be evaluated in this article, or claim that may be made by its manufacturer, is not guaranteed or endorsed by the publisher.

References

1. Yamaguchi T, Aihara A, Mashiko S, Kurosawa E, Oizumi T, Yamagata T, et al. Exacerbation of delirium and epileptic seizures in an older man with idiopathic Parkinson's disease due to multiple prescriptions: a case report. *Front Med.* (2024) 11:1415988. doi: 10.3389/fmed.2024.1415988

2. Pradeep P, Kang H, Lee B. Glycosylation and behavioral symptoms in neurological disorders. *Transl Psychiatry*. (2023) 13:154. doi: 10.1038/s41398-023-02446-x

3. Sun Y, Wei C, Cui V, Xiu M, Wu A. Electroencephalography: clinical applications during the perioperative period. *Front Med.* (2020) 7:251. doi: 10.3389/fmed.2020.00251

4. Huang W, Yan G, Chang W, Zhang Y, Yuan Y. EEG-based classification combining Bayesian convolutional neural networks with recurrence plot for motor movement/imagery. *Pattern Recognit.* (2023) 144:109838. doi: 10.1016/j.patcog.2023.109838

5. Kim BH, Choi JW, Lee H, Jo S. A discriminative SPD feature learning approach on Riemannian manifolds for EEG classification. *Pattern Recognit*. (2023) 143:109751. doi: 10.1016/j.patcog.2023.109751

6. Behrouzi T, Hatzinakos D. Graph variational auto-encoder for deriving EEG-based graph embedding. *Pattern Recognit*. (2022) 121:108202. doi: 10.1016/j.patcog.2021.108202

7. Khurshid D, Wahid F, Ali S, Gumaei AH, Alzanin SM, Mosleh MA, et al. deep neural network-based approach for seizure activity recognition of epilepsy sufferers. *Front Med*. (2024) 11:1405848. doi: 10.3389/fmed.2024.1405848

8. Shoeibi A, Khodatars M, Ghassemi N, Jafari M, Moridian P, Alizadehsani R, et al. Epileptic seizures detection using deep learning techniques: a review. *Int J Environ Res Public Health*. (2021) 18:5780. doi: 10.3390/ijerph18115780

9. Wu M, Wan T, Wan X, Fang Z, Du Y. A new localization method for epileptic seizure onset zones based on time-frequency and clustering analysis. *Pattern Recognit*. (2021) 111:107687. doi: 10.1016/j.patcog.2020.107687

10. Thuwajit P, Rangpong P, Sawangjai P, Autthasan P, Chaisaen R, Banluesombatkul N, et al. EEGWaveNet: multiscale CNN-based spatiotemporal feature extraction for EEG seizure detection. *IEEE Trans Ind Inform*. (2021) 18:5547–57. doi: 10.1109/TII.2021.3133307

11. Wagh N, Varatharajah Y. EEG-GCNN: augmenting electroencephalogram-based neurological disease diagnosis using a domain-guided graph convolutional neural network. In: *Proceedings of the Machine Learning for Health NeurIPS Workshop, Vol. 136*. Vancouver, BC: PMLR (2020). p. 367–78.

12. Ho TKK, Armanfard N. Self-supervised learning for anomalous channel detection in EEG graphs: application to seizure analysis. *Proc AAAI Conf Artif Intell*. (2023) 37:7866–74. doi: 10.1609/aaai.v37i7.25952

13. Liu Y, Li Z, Pan S, Gong C, Zhou C, Karypis G. Anomaly detection on attributed networks via contrastive self-supervised learning. *IEEE Trans Neural Netw Learn Syst*. (2021) 33:2378–92. doi: 10.1109/TNNLS.2021.3068344

14. Kirschstein T, Köhling R. What is the source of the EEG? *Clin EEG Neurosci*. (2009) 40:146–9. doi: 10.1177/155005940904000305

15. Shi W, Rajkumar R. Point-GNN: graph neural network for 3D object detection in a point cloud. In: *Proceedings of the IEEE/CVF Conference on Computer Vision and Pattern Recognition*. Seattle, WA: IEEE (2020). p. 1711–9. doi: 10.1109/cvpr42600.2020.00178

16. Zhou K, Huang X, Song Q, Chen R, Hu X. Auto-GNN: neural architecture search of graph neural networks. *Front Big Data*. (2022) 5:1029307. doi: 10.3389/fdata.2022.1029307

17. Yang X, Yang X, Yang J, Ming Q, Wang W, Tian Q, et al. Learning high-precision bounding box for rotated object detection via Kullback-Leibler divergence. *Adv Neural Inf Process Syst*. (2021) 34:18381–94.

18. Bos DO. EEG-based emotion recognition. The influence of visual and auditory stimuli. Comput Sci. (2006) 56:1–17.

19. Suhaimi NS, Mountstephens J, Teo J. EEG-based emotion recognition: a state-of-the-art review of current trends and opportunities. *Comput Intell Neurosci*. (2020) 2020:8875426. doi: 10.1155/2020/8875426

20. Kale GV, Patil VH. A study of vision based human motion recognition and analysis. *Int J Ambient Comput Intell*. (2016) 7:75–92. doi: 10.4018/IJACI.2016070104

21. Da Gama AEF, de Menezes Chaves T, Fallavollita P, Figueiredo LS, Teichrieb V. Rehabilitation motion recognition based on the international biomechanical standards. *Expert Syst Appl*. (2019) 116:396–409. doi: 10.1016/j.eswa.2018.09.026

22. Hu Z, Lee EJ. Human motion recognition based on improved 3-dimensional convolutional neural network. In: *2019 IEEE International Conference on Computation, Communication and Engineering (ICCCE)*. Fujian: IEEE (2019), p. 154–6. doi: 10.1109/ICCCE48422.2019.9010816

23. Zhang F, Wu TY, Pan JS, Ding G, Li Z. Human motion recognition based on SVM in VR art media interaction environment. *Hum-centric Comput Inform Sci*. (2019) 9:1–15. doi: 10.1186/s13673-019-0203-8

24. Pyun KR, Kwon K, Yoo MJ, Kim KK, Gong D, Yeo WH, et al. Machine-learned wearable sensors for real-time hand motion recognition: toward practical applications in reality. *Natl Sci Rev*. (2023) 11:nwad298. doi: 10.1093/nsr/nwad298

25. Zhou H, Yang G, Wang B, Li X, Wang R, Huang X, et al. An attention-based deep learning approach for inertial motion recognition and estimation in human-robot collaboration. *J Manuf Syst*. (2023) 67:97–110. doi: 10.1016/j.jmsy.2023.01.007

26. Akinyemi TO, Omisore OM, Du W, Duan W, Chen X, Yi G, et al. Interventionalist hand motion recognition with convolutional neural network in robot-assisted coronary interventions. *IEEE Sens J*. (2023) 23:17725–36. doi: 10.1109/JSEN.2023.3281009

27. Li X, Liu Y, Zhou X, Yang Z, Tian L, Fang P, et al. Simultaneous hand/wrist motion recognition and continuous grasp force estimation based on nonlinear spectral sEMG features for transradial amputees. *Biomed Signal Process Control*. (2023) 85:105044. doi: 10.1016/j.bspc.2023.105044

28. Li X, Cao X. Human motion recognition information processing system based on LSTM recurrent neural network algorithm. *J Ambient Intell Humaniz Comput*. (2023) 14:8509–21. doi: 10.1007/s12652-021-03614-x

29. Abdullah AS, AlSaif KI. Computer vision system for backflip motion recognition in gymnastics based on deep learning. *J Al-Qadisiyah Comput Sci Math*. (2023) 15:150. doi: 10.29304/jqcm.2023.15.1.1162

30. Mocanu B, Tapu R, Zaharia T. Multimodal emotion recognition using cross modal audio-video fusion with attention and deep metric learning. *Image Vis Comput*. (2023) 133:104676. doi: 10.1016/j.imavis.2023.104676

31. Sun P, De Winne J, Zhang M, Devos P, Botteldooren D. Delayed knowledge transfer: cross-modal knowledge transfer from delayed stimulus to EEG for continuous attention detection based on spike-represented EEG signals. *Neural Netw*. (2025) 183:107003. doi: 10.1016/j.neunet.2024.107003

32. Wang J, Zhang C. Cross-modality fusion with EEG and text for enhanced emotion detection in English writing. *Front Neurorobot*. (2025) 18:1529880. doi: 10.3389/fnbot.2024.1529880

33. Xu M, Shi T, Zhang H, Liu Z, He X. A hierarchical cross-modal spatial fusion network for multimodal emotion recognition. *IEEE Trans Artif Intell*. (2025) :1–10. doi: 10.1109/TAI.2024.3523250

34. Andrew G, Arora R, Bilmes J, Livescu K. Deep canonical correlation analysis. In: *International Conference on Machine Learning*. PMLR (2013), p. 1247–55.

35. Chen Z, Liu C, Ding SX, Peng T, Yang C, Gui W, et al. A just-in-time-learning-aided canonical correlation analysis method for multimode process monitoring and fault detection. *IEEE Trans Ind Electron*. (2020) 68:5259–70. doi: 10.1109/TIE.2020.2989708

36. Chang X, Xiang T, Hospedales TM. Scalable and effective deep CCA via soft decorrelation. In: *Proceedings of the IEEE Conference on Computer Vision and Pattern Recognition*. (2018), p. 1488–97. doi: 10.1109/CVPR.2018.00161

37. Lai D, Wang S, Chong Z, Wu W, Nardini C. Task-oriented attributed network embedding by multi-view features. *Knowl-Based Syst*. (2021) 232:107448. doi: 10.1016/j.knosys.2021.107448

38. Perozzi B, Al-Rfou R, Skiena S. Deepwalk: Online learning of social representations. In: *Proceedings of the 20th ACM SIGKDD International Conference on Knowledge Discovery and Data Mining*. (2014), p. 701–10. doi: 10.1145/2623330.2623732

39. Mikolov T, Chen K, Corrado G, Dean J. Efficient estimation of word representations in vector space. *arXiv*. (2013) [Preprint]. arXiv:1301.3781. doi: 10.48550/arXiv.1301.3781

40. Grover A, Leskovec J. node2vec: Scalable feature learning for networks. In: *Proceedings of the 22nd ACM SIGKDD International Conference on Knowledge Discovery and Data Mining*. New York, NY: ACM (2016), p. 855–64. doi: 10.1145/2939672.2939754

41. Tang J, Qu M, Wang M, Zhang M, Yan J, Mei Q. Line: large-scale information network embedding. In: : *Proceedings of the 24th International Conference on World Wide Web*. Geneva: International World Wide Web Conferences Steering Committee (2015), p. 1067–77. doi: 10.1145/2736277.2741093

42. Cao S, Lu W, Xu Q. Grarep: Learning graph representations with global structural information. In: *Proceedings of the 24th ACM International on Conference on Information and Knowledge Management*. New York, NY: ACM (2015), p. 891–900. doi: 10.1145/2806416.2806512

43. Zheng C, Pan L, Wu P. Attribute augmented network embedding based on generative adversarial nets. *IEEE Trans Neural Netw Learn Syst*. (2021) 34:3473–3487. doi: 10.1109/TNNLS.2021.3116419

44. Fan H, Zhang F, Wei Y, Li Z, Zou C, Gao Y, et al. Heterogeneous hypergraph variational autoencoder for link prediction. *IEEE Trans Pattern Anal Mach Intell*. (2021) 44: 4125–138. doi: 10.1109/TPAMI.2021.3059313

45. Fan H, Zhang F, Li Z. AnomalyDAE: dual autoencoder for anomaly detection on attributed networks. In: *ICASSP 2020-2020 IEEE International Conference on Acoustics, Speech and Signal Processing (ICASSP)*. Barcelona: IEEE (2020), p. 5685–9. doi: 10.1109/ICASSP40776.2020.9053387

46. Wang H, Wang J, Wang J, Zhao M, Zhang W, Zhang F, et al. Graphgan: graph representation learning with generative adversarial nets. *Proc AAAI Conf Artif Intell*. (2018) 32:2508–15. doi: 10.1609/aaai.v32i1.11872

47. Dai Q, Li Q, Tang J, Wang D. Adversarial network embedding. *Proc AAAI Conf Artif Intell*. (2018) 32:2167–74. doi: 10.1609/aaai.v32i1.11865

48. Zhang F, Fan H, Wang R, Li Z, Liang T. Deep dual support vector data description for anomaly detection on attributed networks. *Int J Intell Syst*. (2021) 1:1. doi: 10.1002/int.22683